Obrabotka metallov (tekhnologiya, oborudovanie, instrumenty) = Metal Working and Material Science. 2023 vol. 25 no. 4 pp. 74–89
ISSN: 1994-6309 (print) / 2541-819X (online)
DOI: 10.17212/1994-6309-2023-25.4-74-89

NSTU NETI

Obrabotka metallov -
Metal Working and Material Science

Journal homepage: http://journals.nstu.ru/obrabotka_metallov

Milling martensitic steel blanks obtained using additive technologies

Nikita Martyushev [1, a, *], *Victor Kozlov* [1, b], *Mengxu Qi* [1, c], *Andrey Baginskiy* [1, d], *Zeli Han* [1, e], *Aleksandr Bovkun* [2, f]

[1] National Research Tomsk Polytechnic University, 30 Lenin Avenue, Tomsk, 634050, Russian Federation
[2] Irkutsk National Research Technical University, 83 Lermontova st., Irkutsk, 664074, Russian Federation

[a] https://orcid.org/0000-0003-0620-9561, martjushev@tpu.ru; [b] https://orcid.org/0000-0001-9351-5713, kozlov-viktor@bk.ru;
[c] https://orcid.org/0000-0003-3738-0193, mensyuy1@tpu.ru; [d] https://orcid.org/0000-0002-1544-6406, bagin@tpu.ru;
[e] https://orcid.org/0000-0001-6502-6541, hanzelizy@gmail.com; [f] https://orcid.org/0000-0002-0623-4284, Bovas87@yandex.ru

ARTICLE INFO

Article history:
Received: 14 July 2023
Revised: 24 July 2023
Accepted: 11 October 2023
Available online: 15 December 2023

Keywords:
Electron-beam surfacing
Additive technologies
Martensitic stainless steel
Cutting forces
Processing modes
Milling

Funding
This research was supported by TPU development program.

Acknowledgements
Research were partially conducted at core facility "Structure, mechanical and physical properties of materials".

ABSTRACT

Introduction. In recent years, more attention has been paid to additive wire printing technologies. Due to the peculiarities of printing with wire, the hardness of the workpiece is significantly higher than with traditional forging. An increase in hardness leads to an increase in cutting force. **The aim of the work** is to study the cutting force during milling workpieces of stainless steel *0.4 C-13 Cr* obtained by electron-beam surfacing. **Research Methods** The specimens were obtained by surfacing wire from martensitic stainless steel *0.4 C-13 Cr*. The microstructure of the specimens was studied in this work. The main attention was paid to the study of cutting forces during the processing of specimens. The work **investigate** specimens obtained by electron-beam surfacing with *0.4 C-13 Cr* steel wire. The cutting forces arising during milling of these specimens are determined. To carry out the research work, a standard methodology for conducting experiments to determine cutting forces was chosen. However, to determine the forces Pz and Py, a four-flute (z = 4) milling cutter was used and the milling width was less than 2 mm. **Results and discussion.** The structure of the specimens obtained by electron-beam surfacing is tempered martensite. It is established that high-speed milling, high-efficiency milling and conventional milling are suitable for processing such workpieces. For processing thin-walled workpieces made of martensitic stainless steel after its manufacture by the method of electron-beam surfacing, it is necessary to use only carbide cutters with a diameter of at least 12 mm. The cutting modes obtained in the study make it possible to reduce the temperature of the cutting edge, cutting force and bending of a low-rigid end mill. So, in the course of the study, it was possible to select modes that reduce the vibration of the machine-device-tool-part system.

For citation: Martyushev N.V., Kozlov V.N., Qi M., Baginskiy A.G., Han Z., Bovkun A.S. Milling martensitic steel blanks obtained using additive technologies. *Obrabotka metallov (tekhnologiya, oborudovanie, instrumenty) = Metal Working and Material Science*, 2023, vol. 25, no. 4, pp. 74–89. DOI: 10.17212/1994-6309-2023-25.4-74-89. (In Russian).

Introduction

The development of science and industry leads to the emergence and active development of new technologies. Such technologies are also emerging in the area of the processing and manufacturing of metal parts and blanks. One of the promising modern technologies used for manufacturing parts is additive technology. Additive technologies do not have very high productivity; the cost of manufacturing parts using this technology is also quite high. One of the directions in the development of additive technologies is the

*** Corresponding author**
Martyushev Nikita V., Ph.D. (Engineering), Associate Professor
National Research Tomsk Polytechnic University,
30 Lenin Avenue,
634050, Tomsk, Russian Federation
Tel.: +7 (3822) 60-62-85, **e-mail:** martjushev@tpu.ru

printing of specimens using metal surfacing. This technology significantly reduces the production time of the workpiece and reduces the cost of its production. This is due to the fact that instead of powder, surfacing wire is used during printing, the cost of which is significantly lower. However, a significant disadvantage of printed specimens is the low quality of the surface and such specimens require additional machining. Due to the peculiarity of this technology associated with the cooling of printed parts, its hardness is higher than when using forging or casting. This is especially evident when manufacturing parts made of martensitic stainless steels. These steels are quite inexpensive and are widely used, including for surfacing.

When forming a part using a layer-by-layer surfacing, a new layer is applied to the previous one. The previous one is reheated and quickly cooled again. Since the critical cooling rate of martensitic steels is not high, a martensitic structure of high hardness is formed. The research conducted by the authors in [2, 3] confirms this fact. The layer-by-layer laser surfacing of the powder imparts different mechanical properties throughout the cross-section of the printed workpieces. The grain size, porosity and, accordingly, mechanical properties depend on the direction in which it is measured. In [4], the authors also showed that the properties of the products printed using additive technologies are different in different directions. The authors also showed that this could be partially corrected by heat treatment. Nevertheless, such correction requires additional costs for an additional operation. Similar results are shown in [5] demonstrating that thermal cycling of individual areas during printing may initiate internal stresses occurrence within the printed workpiece. The work [5] states that a hard-to-process crust (750 HV) was formed on the surface of *0.4 % C-13 % Cr* steel specimens during *SLM*.

When printing with wire (*WAAM*), the bottom layer recrystallizes while the next layer is applied to it. In this case, a structure, consisting of elongated grains of ferrite and fine-grained acicular martensite, is formed in the matrix upper layer. This structure is formed instead of the spatial periodicity of martensite laths within equiaxed ferrite grains in the inner layers. The martensite content gradually increases proportionally to the distance from the base metal [6].

The operating equipment conditions largely determine the process of forming a workpiece using the wire surfacing. These are parameters such as the temperature of the substrate, the trajectory of movement [7], etc. However, even under optimal conditions, various defects in the structure of the material may still appear (surface hardening, inhomogeneity, etc.). The *WAAM* technology is one of the additive technologies. When printing workpieces using the *WAAM* technology, the workpieces with heterogeneous structure and mechanical properties are also obtained. Another disadvantage of the *WAAM* technology is a poor surface quality. After the workpiece is manufactured, subsequent machining is required to obtain the desired geometric tolerances and surface properties [8]. When machining such workpieces, it is necessary to consider these features. Processing of workpieces obtained from stainless steels using the *WAAM* method on a milling machine is possible with fairly high productivity [9]. However, a significant tool wear is observed when milling the *WAAM* part. This occurs despite the fact that the tool and milling parameters were selected based on the manufacturer's recommendations intended for processing a given material.

The heterogeneous microstructure formed in the specimen obtained by the *WAAM* technology leads to a significant deterioration in its machinability. This is due to complex thermal cycles occurring during printing. The authors of [10] demonstrated the difficulties that arise when milling the *Ti6Al4V* alloy with an Al_2O_3/Si_3N_4 (sialon) end mill. The authors noted a more significant tool wear when machining the *WAAM* specimens as compared to forged and cast ones.

The wear can be reduced and the tool life may increase by changing the cutting speed and feed [11, 12]. The cryogenic cooling of the cutting tool can also be used.

Another way to reduce the tool wear is to select printing modes that enable the desired surface properties. To overcome the hardness heterogeneity of the printed workpiece, a methodology intended for segregating microhardness data into individual assemblies was developed and tested [13, 14]. Combining various additive printing technologies allows obtaining a more uniform structure. But in general, researchers [15] note that when processing printed workpieces, cutting forces increase in comparison with those of the workpieces produced by traditional methods. The authors of [16] stated that the workpieces produced by additive technologies possessed completely different cutting forces under the same processing conditions.

Down milling is recommended for processing the parts made of the *316L* steel produced by laser additive technologies (*LAM*) [17, 18]. It provides a better surface quality in terms of roughness compared to that of counter-production. Tool wear can be reduced and machining productivity can be increased using ultrasonic vibration milling during down milling [19–23]. At the same time, the work is currently underway to combine additive and subtractive technologies using the same equipment [24]. This improves the manufacturing accuracy, reduces the operating time and tool wear.

The importance of determining the optimal processing modes of workpieces obtained by additive wire printing methods is noted in [25]. Moreover, the standard processing modes are reported not to provide optimal results. In general, the authors of [25–28] also suggest that different positions of the workpiece during 3D printing generate different properties during printing. The vertically manufactured workpieces are cooled more slowly than the horizontally located ones. As a result, depending on the workpiece location during printing, its properties will be different. This will also affect the processing modes. Therefore, when assigning subtractive processing modes, it is important to know the workpiece manufacturing specifics. This will directly affect the quality of processing and tool wear. This is especially important for the parts made by electron-beam printing (*EBW*). The printing blanks using the *WAAM* method is more widespread due to its low cost. The *EBW* method produces more precise and critical parts. Such parts should have higher accuracy. Therefore, for workpieces manufactured by the *EBW* method, it is extremely important to study the features of subsequent retractive processing. An analysis of the literature shows that there are works devoted to the properties of differently oriented printed specimens. Nevertheless, there are practically no works showing how much these changes in properties for differently oriented printed specimens affect the modes of subtractive processing. There are practically no works devoted to the processing of the workpieces printed using the *EBW* method.

There are very few works devoted to the subtractive processing of the workpieces obtained by electron-beam printing. Therefore, the topic of selecting optimal modes of processing the workpieces manufactured using *WAAM* (wire surfacing) methods is very relevant.

The aim of this work is to use the experimental work to determine the patterns of changes in forces when milling the workpieces made of the stainless steel *0.4 % C-13 % Cr*, manufactured by electron-beam surfacing.

Materials and methods

To conduct the research on milling, specimens were obtained using the electron-beam wire surfacing technology. 10 specimens were printed for the research. 5 specimens were used for down milling and 5 specimens underwent up milling. The dimensions of the specimens were 14×70×15 mm (height × width × length). The specimens under study were printed using steel wire, the chemical composition of which is given in Table 1.

Table 1

The chemical composition of martensitic steel

C	*Mn*	*Si*	*Ni*	*Cr*	*P*	*S*	*Fe*
0.40	0.49	0.54	0.50	13.1	0.020	0.016	balance

Manufacture of the specimens using an electron beam installation

The specimens were printed using an electron-beam (*EBW*) wire surfacing machine. The installation was developed and manufactured at *Tomsk Polytechnic University* (fig. 1).

The accelerating voltage of the *EBW* installation is 40 kV and it remains unchanged. The current variation range is 0–200 mA. The initial material intended for producing a workpiece using the EBW method is the stainless steel *0.4 % C-13 % Cr* wire with a diameter of 1.2 mm. The general scheme for printing the specimens is shown in fig. 2.

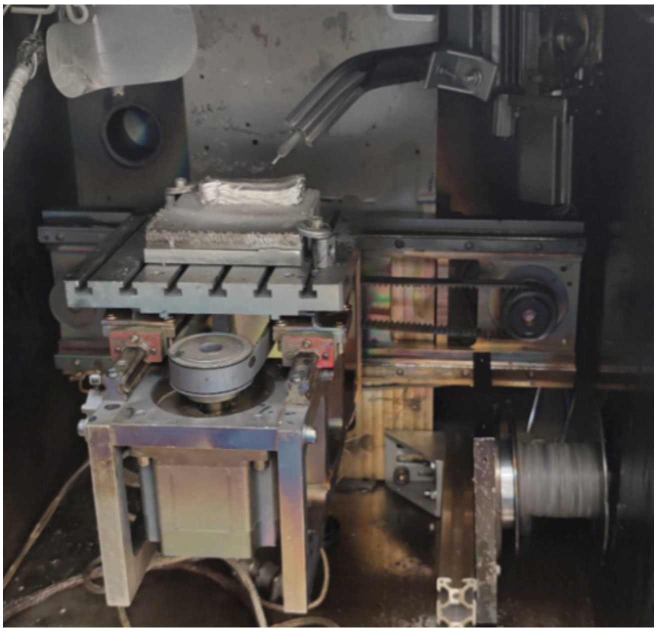

Fig. 1. General view of the working chamber of the electron-beam wire surfacing installation

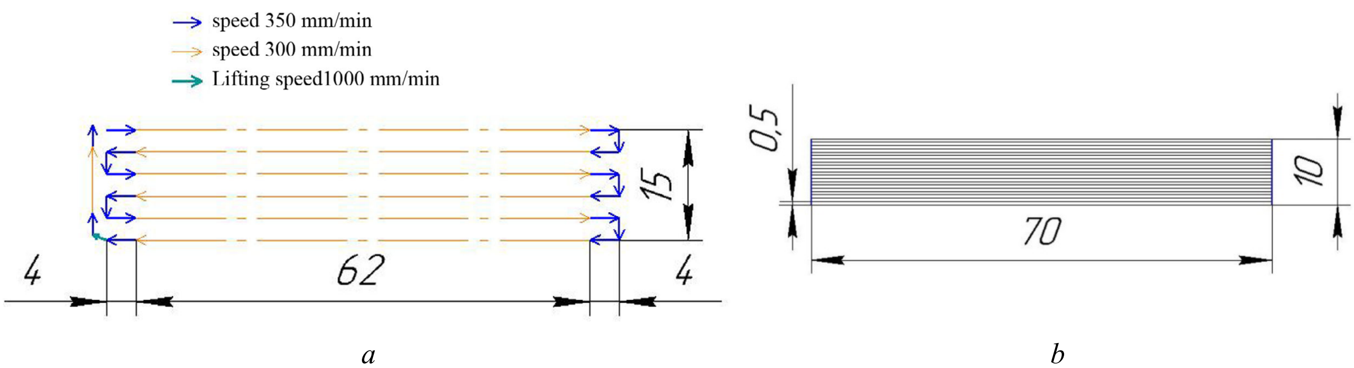

Fig. 2. Scheme for printing a specimen: pattern for printing one horizontal layer (*a*); print pattern in the vertical direction (*b*)

When printing the specimens, the following modes were used:
- circular beam scan: 3.0–5.0 mm;
- wire feed angle: 45.0°;
- beam current: 30 mA;
- wire feed speed: 700 mm/min.

When printing, the same material was used as the substrate material as for the wire – stainless steel *0.4 % C-13 % Cr*. Printing was carried out in a vacuum at pressure 5×10^{-3} Pa.

The study of the microstructure of the obtained specimens

The microstructure of the specimens was detected using an etchant. Its composition was a mixture of concentrated nitric HNO_3 (67 wt. %) and hydrochloric *HCl* (33 wt. %) acids. The ratio of acids was 1:3 by volume. The microstructure was studied using a *MMP-1* microscope (*BIOMED*).

Study of cutting forces during milling

An *CNC* machine *CONCEPTMill 155* (*EMCO*) was used to mill the specimens. Cutting forces were determined using a *Kistler 9257B* dynamometer (Switzerland). The directions of the measured forces F_x, F_y and F_z displayed on the monitor of the *Kistler* dynamometer, correspond to the forces P_h, P_v and P_x during milling. In addition, the forces F_z, F_y approximately correspond to the tangential P_z and radial P_y forces during penetration and when the tooth leaves contact, if t is equal to half the cutter diameter

To carry out the research work, a standard methodology used for conducting experiments to determine cutting forces was chosen. However, to determine the forces P_z and P_y, we made a number of deviations from this technique. A four-flute ($z = 4$) cutter was used; the milling width was less than 2 mm. The milling depth t was slightly less (0.2 mm) than half the cutter diameter d ($t \approx 0.5 \cdot d - 0.2$). This deviation from the standard approach made it possible to calculate the components of the normal N and tangential F forces acting on the front surface of the cutter tooth using certain forces P_z and P_y. In this case, the rake angle was taken into account.

DynoWare software was used to analyze the data. The sensitivity of the dynamometer is 7.5 N, its measurement error is ±0.005 %. The scatter in measuring cutting forces was no more than 15 %. This error is due to the wear of the milling cutter. If there is wear, it is necessary to make a reconfiguration. However, it is very difficult to ensure the accuracy of the adjustment to the required width and depth of milling, even with a slight wear of the cutter during experiments. Carbide end mills produced by *GESAC* (China) were chosen as the tool. The hard alloy consisted mainly of tungsten carbides and a cobalt binder (~8 %). Its parameters are given in table 2. The rear angle was 5º, the rake angle amounted to 7º. We used cutters covered with a coating, the characteristics of which are given in table 3. The choice of the cutters with such a coating is determined by the processing conditions. In the experiments we used up and down dry milling. Down milling was carried out with a 4-tooth cutter of $d = 8$ mm, milling width of which was $B = 2$ mm, the spindle speed was $n = 500$ rpm, the feed was $s_m = 104$ mm/min. A large feed value was chosen in order to test the selected tool in extreme operating conditions. Up milling was also carried out with a 4-tooth cutter of $d = 8$ mm at $B = 2$ mm, $n = 500$ rpm, $s_m = 28$ mm/min. When choosing cutting modes, we proceeded from the experience of the work performed by the authors in [28].

Table 2

The main parameters of the milling cutters used

Factory marking	Coating	Diameter, D, mm	Helical flute angle, ω, °	Number of teeth, z
UP210-S4-08020	*AlCrSiN*	8	35	4

Table 3

The main parameters of the coating of the milling cutters used

Coating	HV0.05	μ	T
AlCrSiN	3,300	0.4	1,100

Results and discussion

Obtaining specimens by electron-beam surfacing and studying its microstructure

At the first stage of the work, we prepared specimens intended for subsequent machining. Since the technology used for printing specimens by means of an electron beam by surfacing the wire is quite new, there are practically no standard modes for producing specimens. Printing modes are mainly depend on the material being printed and the geometric dimensions of the specimens. We presented the technology for selecting the printing modes for the stainless steel *0.4 % C-13 % Cr* in more detail in [28]. The beam current value was ranging within some limit to determine the optimal printing modes. During the experiments, 6 different beam current values were used. The value at which the highest quality specimen was obtained gaining the fewest defects and a smooth surface was then used to obtain the remaining specimens.

Manufacturing the specimens using electron-beam surfacing

In this work, 5 experimental specimens were printed using the electron-beam 3D wire printing technology. As a result of the preliminary work, the optimal value of the beam current was determined to be 30 mA (fig. 3).

Fig. 3. A specimen obtained by electron-beam surfacing with a *0.4 C-13 Cr* steel wire

The first printed layer has the fastest cooling rate. If the beam current is too high, this leads to the melt-through of not only the wire, but also of the substrate material. As a result, a hole appears at the border of the printed specimen. Printing the next layer will not be possible. As the beam current decreases, the print path length increases. As the number of the printed layers increases, the cooling rate decreases and the overall temperature of the specimen increases. Based on this, when printing the specimens, the optimal printing modes were determined under which it was possible to form the workpiece layer by layer. This is a beam current of 30 mA and a wire feed of 700 mm/min [28].

Study of the microstructure of the printed specimens

Traditional methods of forming blanks (forging, casting) ensure a completely martensitic structure for the stainless steel *0.4 % C-13 % Cr*. When using additive technologies, austenite and δ-ferrite can form in such steel. In the course of our work, we studied the microstructure of steels.

As shown in fig. 4, the printed specimens have a dense structure. There are no cracks at the interlayer boundaries and there is no boundary of the molten pool. The microstructure of the manufactured specimens is similar to the microstructure of the steel *0.4 % C-13 % Cr* after quenching and low tempering [29–33]. Martensite has a needle-like structure. This behavior is attributed to the high cooling rate during solidification in electron-beam additive manufacturing, which facilitates the phase transformation of austenite to martensite. These randomly oriented martensitic needles are much smaller than the martensitic needles formed during the casting and quenching of stainless steel *0.4 % C-13 % Cr* [26, 27]. When additively printing a specimen, the heat coming from the applied new layer affects the previously printed ones. The underlying layers below the printed layer are heated above the austenitizing temperature. The previously formed martensite transforms into austenite and, after cooling, retained austenite and martensite form again. However, if the temperature is insufficient and below the austenitization temperature, then the process of martensite tempering occurs, the retained austenite again turns into martensite.

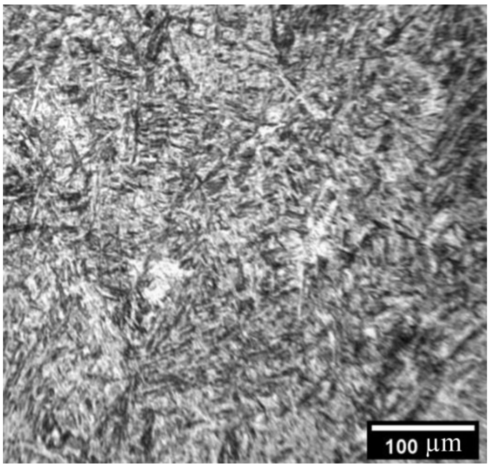

a

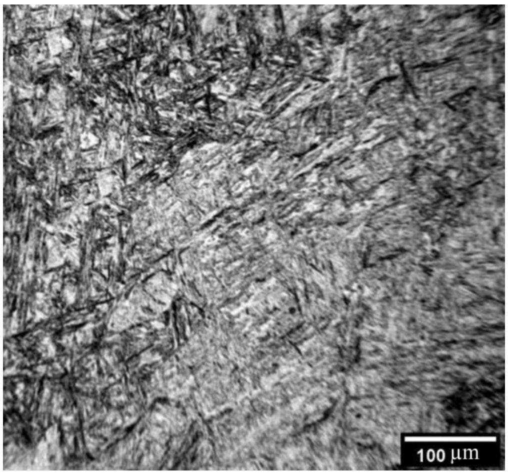

b

Fig. 4. Microstructure of the specimens: the area near the edge of the specimen (*a*); the central part of the specimen (*b*)

Study of cutting forces when machining the specimens

At the third stage of our work, we conducted a study of the cutting forces arising during milling of the printed specimens. When processing the printed specimens, the greatest attention in this work was paid to the component forces P_h and P_v (fig. 5, 6). This is because the P_x force is small relative to other forces. It is directed along the axis of the cutter. This is the direction of the highest rigidity of the cutter (fig. 6). The radial direction is the direction of the lowest rigidity used for the end mill. Based on this, the force P_y acting radially on the cutter axis leads to vibration.

During the study, we constructed graphs of changes occurring in the cutting forces during milling with a four-flute cutter for up and down milling processes.

Up milling process

When up milling with a four-tooth cutter having a diameter of 8 mm at $t = 3.8$ mm, the change in the components of the cutting forces as a function of time τ (s) is shown in fig. 7. The cutter diameter that is slightly less than 4 mm was taken to ensure that the next tooth had not yet started cutting. The graph shows the forces generated during one full revolution of the cutter. The curves of the main cutting force components P_h and P_v show four clear peaks. These peaks correspond to the work of each of the four cutter teeth. The force increases when the tooth cuts into the workpiece and the force decreases when the tooth leaves the cutting zone.

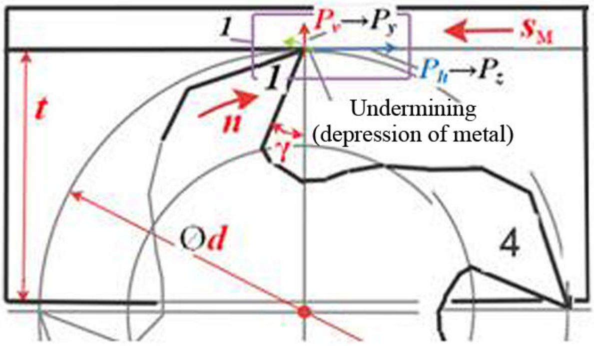

a

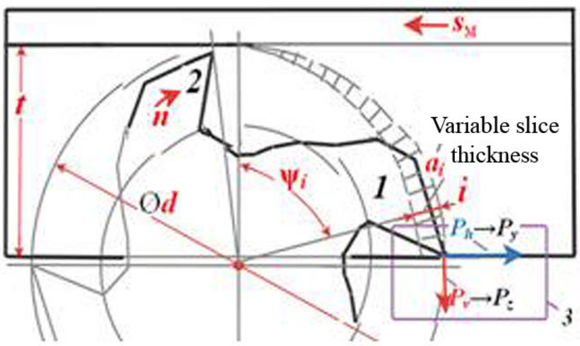

b

Fig. 5. The direction scheme of the components of the cutting force in asymmetric up end milling with a four-tooth end mill with a diameter of $d = 8$ mm at a milling depth of $t = d/2 - 0.2$ mm $= 3.8$ mm: when tooth No.1 enters the workpiece (the previous tooth No.4 is already out of contact) (*a*); when tooth No.1 leaves contact with the workpiece (the next tooth No.2 has not yet come into contact with the workpiece) (*b*)

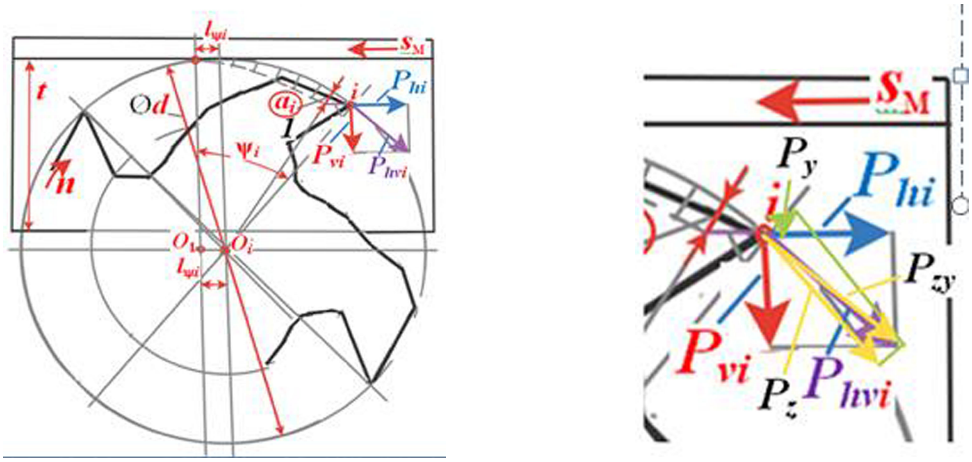

a *b*

Fig. 6. The direction scheme of the components of the cutting force in asymmetric up end milling in the top view: the position of the cutter tooth at a central angle $\psi \approx 50^o$ from the point of contact to the considered position (*a*); large diagram of the action of the components P_{vi} and P_{hi}, as well as P_z and P_y and its resulting P_{hvi} and P_{zy} at $\psi \approx 50^o$ (*b*)

The axial component P_x changes slightly throughout the entire cycle (fig. 7, the range is between numbers 1 and 5), because along the end part, three teeth are in contact with the workpiece almost immediately having a four-flute cutter and milling depth of $t \approx d/2$ (fig. 5, *a*, *b*) when decreasing the milling depth of $t < 0.2d$. That is, if the milling depth t is less than the cutter flute depth h, only one tooth will be in constant contact with the workpiece. This will cause large changes in the value of the P_x component as the cutter rotates.

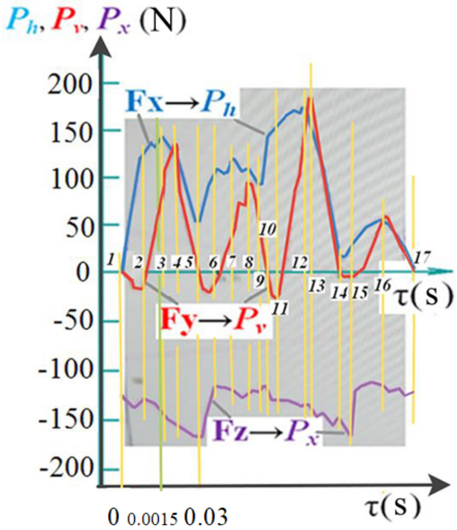

Fig. 7. Graphs of force changes during milling when turning a sharp cutter for one revolution. Up milling with a 4-tooth cutter $d = 8$ mm, $t = 3.8$ mm, $B = 2$ mm, $n = 500$ rpm, $sm = 28$ mm/min, specimen No.1 – carbide

The operating time of one tooth is $t = d/2$ and a four-tooth cutter ($z = 4$) has $\tau_{1\ tooth} = 60/(4 \cdot n)$ (s). The graph of changes in the magnitude of the components P_h P_v and P_x of the cutting force (fig. 7) shows that there is a non-synchronous change in its value. When analyzing changes in the milling forces, one should keep in mind that the *Kistler* dynamometer is installed across the milling table (perpendicular to the longitudinal feed of the table s_m), and the workpiece is installed with its long part across the dynamometer, i.e., parallel to the direction of the longitudinal feed of the table s_m. The workpiece is behind the cutter when viewed from the operator's side.

When a tooth cuts into a workpiece (fig. 7, the range is between numbers 1 and 2), the cutter tooth with its rounded cutting edge pushes the workpiece away from the axis of rotation of the cutter. That means that a component force P_v cut appears with a negative sign (in the signal processing program using the *Kistler* dynamometer, the sensors are "wired" and the positive sign of the force F_y (P_v during milling) will be when the force is applied towards the operator, i.e. as in turning).

At the same time, the component force P_h of the cut acts with a positive sign, i.e., the cutter tooth pushes the workpiece in the direction opposite to the direction of the counter feed s_m (fig. 8). The positive sign of the force F_x (P_h during milling) on the monitor will be when the force is applied from left to right, i.e. as in turning.

When the tooth rotates further (fig. 7, the range is between numbers 2 and 3), the force P_v acts in the positive direction of the *OY* axis. That is, the cutter tooth attracts the workpiece to the axis of rotation of the cutter due to the positive main rake angle γ (fig. 8, but the position of the cutter after the workpiece is

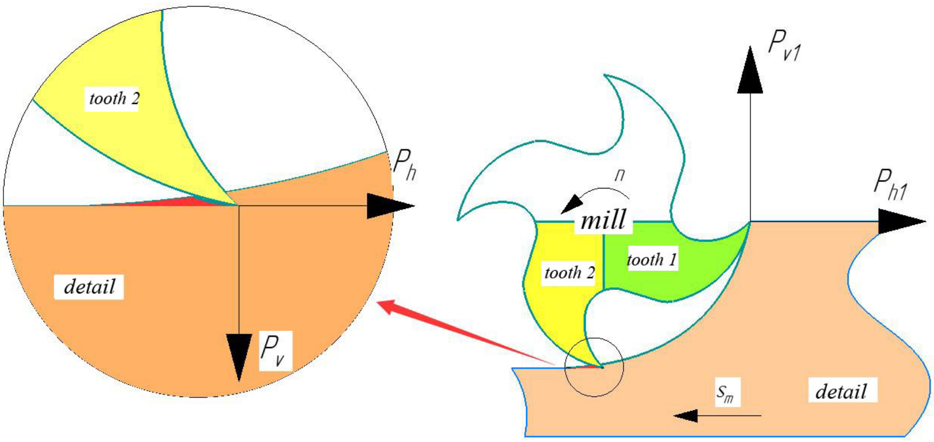

Fig. 8. Component forces acting on the workpiece during up milling with a sharp cutter (the position of the cutter after the workpiece is shown in the top view)

shown in the top view). The component force P_h continuously increases as the cutter tooth rotates, since the cut thickness $a_i = s_z \cdot \sin\psi_i$ increases (fig. 7, the range is between numbers 2 and 3).

As the cutter tooth rotates through an angle ψ, the cut thickness a increases, the direction of the components P_z and P_y of the cutting force also changes (fig. 9, but the position of the cutter after the workpiece is shown in the top view). As the cut thickness a increases, the force P_z increases more intensively than the force P_y does, since this component is "responsible" for cutting the chips. When the cut thickness increases, the force P_y practically should not change including a sharp cutting wedge due to the low friction coefficient on the front surface of the cutter tooth. Changing the action direction of the forces P_z and P_y when turning the cutter through an angle ψ leads to the fact that the component P_v increases. And the component P_h begins to decrease, on the contrary, due to the rotation of the greatest force *Pz* towards the *OY* axis, i.e. it increases the force P_v further instead of P_h (fig. 7, the range is between numbers 3 and 4).

A further rotation of the cutter leads to a decrease in the cut thickness a_i during the period when the tooth leaves contact with the workpiece, which causes a decrease in the components P_z and P_y, and therefore the components P_h and P_v (fig. 7, the range is between numbers 4 and 5). The decrease in these components

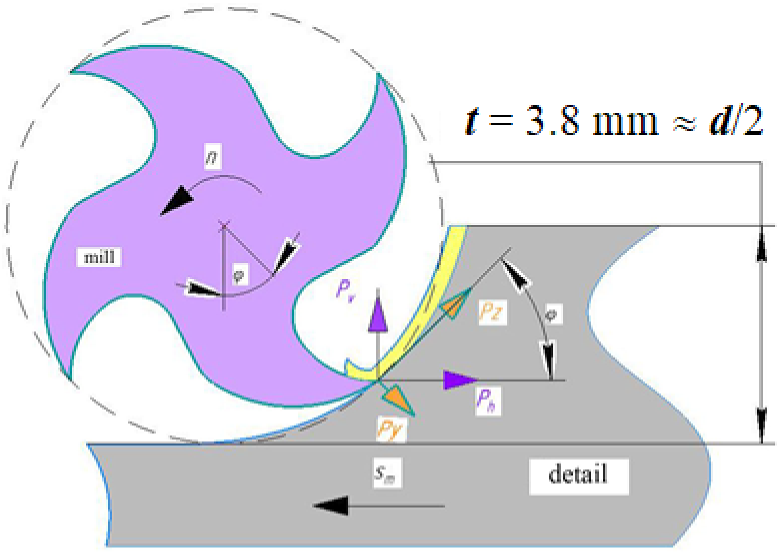

Fig. 9. Force components (P_y, P_z) obtained after decomposing the milling force (P_h, P_v) into a direction towards the cutter axis and a tangential direction, i.e. tangent to the direction of rotation of the cutter (the position of the cutter after the workpiece is shown in top view)

does not occur as quickly as the decrease in cut thickness does at the end of the cut with a tooth, because elastic deformation of the *MDTP* system (machine-device-tool-part) does not allow it to be as sharply as theoretically expected. We believe that with an increase in the *MDTP* system rigidity, and, above all, with an increase in the end mill rigidity as the most flexible element, there will be a more rapid decrease in the forces at the end of the cutter tooth operation.

A negative value of the sign of the force P_x (P_x = –120…–170 N) indicates the desire of the cutter to lift the workpiece, which is associated with a positive inclination angle of the cutter teeth of ω = 40º.

An increase of the force P_x in the negative direction within the range of numbers 2–5 (fig. 7) is associated with an increase in the cut thickness when turning the cutter. Moreover, a decrease in the range of numbers 5–6 is associated with a decrease in the cut thickness at the end of the cycle of cutting the allowance with the tooth in question.

During further rotation of the cutter, the next cutter tooth begins to cut into the workpiece, so the cycle of changing the component forces is repeated (fig. 7, the range is between numbers 5 and 9).

Down milling process

When cutting a tooth into the workpiece (fig. 10, the range is between numbers 1 and 2), the cut thickness a quickly increases to the maximum value a_{max}, so the component force P_h quickly increases to the maximum value. And P_v also quickly increases in the negative direction of the *OY* axis of the dynamometer (the cutter, with its rounded cutting edge and its rear surface, pushes the workpiece away from the axis of the cutter).

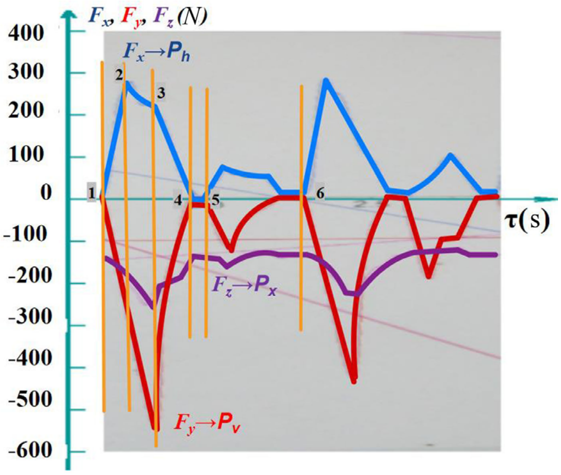

Fig. 10. Graphs of force changes during milling when turning a sharp cutter for one revolution. Down milling with a 4-tooth cutter d = 8 mm, t = 4 mm, B = 2 mm, n = 500 rpm, sm = = 104 mm/min, specimen No.1 – carbide

Since the feed rate s_m = 104 mm/min is very high, i.e. the cut thickness a is large, the force P_y acting in the radial direction towards the cutter axis also includes a normal load acting from the rear surface of the tooth when cutting-in. Under the influence of forces P_y and P_z, the component P_v continues to increase in a negative direction due to the high feed and movement of the cutter tooth to continue cutting. Since the cut thickness decreases during down milling, the undercutting of the metal under the cutting edge increases, but not as intensely as it does during up milling because of the presence of chips on the front surface of the cutter tooth. On the contrary, the P_h component at this time begins to decrease due to a decrease in the slice thickness and, accordingly, a decrease in the force P_z, and in addition, it rotates towards the *OY* axis, i.e., it acts more on the force P_v, and not on the P_h (fig. 10, the range is between numbers 2 and 3).

Further rotation of the cutter leads to a further reduction in the cut thickness a to zero, which causes a decrease in the components P_z and P_y, and therefore the components P_h and P_v (fig. 10, the range is between numbers 3 and 4).

Due to the elastic deformation of the *MDTP* system, under the influence of force P_v, the cutter is repelled from the machined surface, which is why the depth of cut does not reach the specified value, and, in turn, this leads to a reduction in the time of milling with one tooth of the workpiece. In fig. 10 in the range between the numbers 4 and 5 the forces are equal to zero.

As well as the change in force, P_x during up milling, P_x during down milling fluctuate up and down depending on the change in the cutting thickness *a*, and these changes are small. A negative value of the sign of the force P_x indicates the tendency of the cutter to lift the workpiece, which is associated with a positive angle of of the cutter teeth inclination ω = 40º.

During further rotation of the cutter, the next cutter tooth begins to cut into the workpiece, so the cycle of changing the component forces is repeated (fig. 10, the range is between numbers 5 and 6). However, due to the elastic deformation of the *MDTP* system and the slight radial runout of the teeth, the maximum force of each cycle is not the same.

As a result of the experimental work, the forces acting on the tool when processing specimens from heat-resistant steel obtained by the *EBW* wire method are determined. Patterns of changes in cutting forces during cutting with one tooth are also obtained. Important results include determining the change in the direction of the lateral component of the cutting force P_v. Since the presence of a gap in the screw pair of the transverse feed of the machine leads to vibrations, it should be reduced to a minimum. Knowing the P_h feed force obtained from the results of the tests allows calculating the necessary workpiece clamping force. This is especially important when the workpiece has low rigidity. These results are important for manufacturing enterprises when processing workpieces obtained by the *EBW* wire method.

Conclusion

The cutting forces are studied by milling the rectangular specimens produced by electron-beam surfacing of the martensitic stainless steel. Based on the experiments, the following main conclusions are drawn:

1. The structure of the specimens printed by electron-beam surfacing corresponds to tempered martensite.

2. The magnitude of the resulting cutting force P_{hv} for up and down milling is almost the same. But the cutting force in the feed direction P_h during up milling is significantly greater than that taking place during down milling, and the lateral force P_v during up milling is significantly less than that arising during down milling. Based on the mentioned, when processing thin-walled parts, down milling should be used.

3. In this work, using a slight deviation from the standard method of measuring the cutting forces, the dependences of the changes in forces P_z and P_y during the operation of the cutter are obtained. These data allow constructing diagrams of contact stresses involving known physical components on the front surface of the tooth. The standard methodology does not provide such data. This is especially important for the process of designing a new tool. This allows calculating the tool in terms of the work devoted to the stainless steel *0.4 % C-13 % Cr*. The forces P_z and P_y acting on the cutter tooth are determined. As a continuation of this work, it is planned to determine the forces P_z and P_y for titanium alloys obtained by the *EBW* wire surfacing.

References

1. Alvarez L.F., Garcia C., Lopez V. Continuous cooling transformations in martensitic stainless steels. *ISIJ International*, 1994, vol. 34 (6), pp. 516–521. DOI: 10.2355/isijinternational.34.516.

2. Kazemipour M., Lunde J.H., Salahi S., Nasiri A. On the microstructure and corrosion behavior of wire arc additively manufactured AISI 420 stainless steel. *TMS 2020 149th Annual Meeting & Exhibition Supplemental Proceedings*. Springer, 2020, pp. 435–448. DOI: 10.1007/978-3-030-36296-6_41.

3. Liverani E., Fortunato A. Additive manufacturing of AISI 420 stainless steel: Process validation, defect analysis and mechanical characterization in different process and post-process conditions. *The International Journal of Advanced Manufacturing Technology*, 2021, vol. 117 (3–4), pp. 809–821. DOI: 10.1007/s00170-021-07639-6.

4. Saeidi K., Zapata D.L., Lofaj F., Kvetkova L., Olsen J., Shen Z., Akhtar F. Ultra-high strength martensitic 420 stainless steel with high ductility. *Additive Manufacturing*, 2019, vol. 29, p. 100803. DOI: 10.1016/j.addma.2019.100803.

5. Krakhmalev P., Yadroitsava I., Fredriksson G., Yadroitsev I. In situ heat treatment in selective laser melted martensitic AISI 420 stainless steels. *Materials & Design*, 2015, vol. 87, pp. 380–385. DOI: 10.1016/j.matdes.2015.08.045.

6. Ge J., Lin J., Chen Y., Lei Y., Fu H. Characterization of wire arc additive manufacturing 2Cr13 part: Process stability, microstructural evolution, and tensile properties. *Journal of Alloys and Compounds*, 2018, vol. 748, pp. 911–921. DOI: 10.1016/j.jallcom.2018.03.222.

7. Manokruang S., Vignat F., Museau M., Limousin M. Process parameters effect on weld beads geometry deposited by Wire and Arc Additive Manufacturing (WAAM). *Advances on Mechanics, Design Engineering and Manufacturing III. JCM 2020*. Springer, 2021, pp. 9–14. DOI: 10.1007/978-3-030-70566-4_3.

8. Grzesik W. Hybrid additive and subtractive manufacturing processes and systems: a review. *Journal of Machine Engineering*, 2018, vol. 18 (4), pp. 5–24. DOI: 10.5604/01.3001.0012.7629.

9. Lopes J.G., Machado C.M., Duarte V.R., Rodrigues T.A., Santos T.G., Oliveira J.P. Effect of milling parameters on HSLA steel parts produced by Wire and Arc Additive Manufacturing (WAAM). *Journal of Manufacturing Processes*, 2020, vol. 59, pp. 739–749. DOI: 10.1016/j.jmapro.2020.10.007.

10. Dang J., Zhang H., Ming W., An Q., Chen M. New observations on wear characteristics of solid Al_2O_3/Si_3N_4 ceramic tool in high speed milling of additive manufactured Ti6Al4V. *Ceramics International*, 2020, vol. 46 (5), pp. 5876–5886. DOI: 10.1016/j.ceramint.2019.11.039.

11. Bordin A., Bruschi S., Ghiotti A., Bariani P.F. Analysis of tool wear in cryogenic machining of additive manufactured Ti6Al4V alloy. *Wear*, 2015, vol. 328–329, pp. 89–99. DOI: 10.1016/j.wear.2015.01.030.

12. Milton S., Morandeau A., Chalon F., Leroy R. Influence of finish machining on the surface integrity of Ti6Al4V produced by selective laser melting. *Procedia CIRP*, 2016, vol. 45, pp. 127–130. DOI: 10.1016/j.procir.2016.02.340.

13. Keist J.S., Palmer T.A. Development of strength-hardness relationships in additively manufactured titanium alloys. *Materials Science and Engineering: A*, 2017, vol. 693, pp. 214–224. DOI: 10.1016/j.msea.2017.03.102.

14. Tascioglu E., Kaynak Yu., Poyraz Ö., Orhangül A., Ören S. The effect of finish-milling operation on surface quality and wear resistance of Inconel 625 produced by selective laser melting additive manufacturing. *Advanced Surface Enhancement. INCASE 2019*. Springer, 2020, pp. 263–272. DOI: 10.1007/978-981-15-0054-1_27.

15. Montevecchi F., Grossi N., Takagi H., Scippa A., Sasahara H., Campatelli G. Cutting forces analysis in additive manufactured AISI H13 alloy. *Procedia CIRP*, 2016, vol. 46, pp. 476–479.

16. Hojati F., Daneshi A., Soltani B., Azarhoushang B., Biermann D. Study on machinability of additively manufactured and conventional titanium alloys in micro-milling process. *Precision Engineering*, 2020, vol. 62, pp. 1–9. DOI: 10.1016/j.precisioneng.2019.11.002.

17. Gong Y., Li P. Analysis of tool wear performance and surface quality in post milling of additive manufactured 316L stainless steel. *Journal of Mechanical Science and Technology*, 2019, vol. 33, pp. 2387–2395. DOI: 10.1007/s12206-019-0237-x.

18. Ni Ch., Zhu L., Yang Zh. Comparative investigation of tool wear mechanism and corresponding machined surface characterization in feed-direction ultrasonic vibration assisted milling of Ti–6Al–4V from dynamic view. *Wear*, 2019, vol. 436, p. 203006. DOI: 10.1016/j.wear.2019.203006.

19. Xiong X., Haiou Z., Guilan W. A new method of direct metal prototyping: hybrid plasma deposition and milling. *Rapid Prototyping Journal*, 2008, vol. 14 (1), pp. 53–56. DOI: 10.1108/13552540810841562.

20. Ahmetshin R., Fedorov V., Kostikov K., Martyushev N., Ovchinnikov V., Rasin A., Yakovlev A. SLS setup and its working procedure. *Key Engineering Materials*, 2016, vol. 685, pp. 477–481. DOI: 10.4028/www.scientific.net/KEM.685.477.

21. Martyushev N., Petrenko Yu. Effects of crystallization conditions on lead tin bronze properties. *Advanced Materials Research*, 2014, vol. 880, pp. 174–178. DOI: 10.4028/www.scientific.net/AMR.880.174.

22. Isametova M.E., Martyushev N.V., Karlina Y.I., Kononenko R.V., Skeeba V.Yu., Absadykov B.N. Thermal pulse processing of blanks of small-sized parts made of beryllium bronze and 29 NK alloy. *Materials*, 2022, vol. 15, p. 6682. DOI: 10.3390/ma15196682.

23. Martyushev N.V., Bublik D.A., Kukartsev V.V., Tynchenko V.S., Klyuev R.V., Tynchenko Y.A., Karlina Y.I. Provision of rational parameters for the turning mode of small-sized parts made of the 29 NK alloy and beryllium bronze for subsequent thermal pulse deburring. *Materials*, 2023, vol. 16, p. 3490. DOI: 10.3390/ma16093490.

24. Cahoon B.W.H., Broughton W.H., Kutzak A.R. The determination of yield strength from hardness measurements. *Metallurgical Transactions*, 1971, vol. 2 (7), pp. 1979–1983. DOI: 10.1007/bf02913433.

25. Abootorabi Zarchi M.M., Razfar M.R., Abdullah A. Influence of ultrasonic vibrations on side milling of AISI 420 stainless steel. *The International Journal of Advanced Manufacturing Technology*, 2013, vol. 66, pp. 83–89. DOI: 10.1007/s00170-012-4307-9.

26. Lou X., Andresen P.L., Rebak R.B. Oxide inclusions in laser additive manufactured stainless steel and their effects on impact toughness and stress corrosion cracking behavior. *Journal of Nuclear Materials*, 2018, vol. 499, pp. 182–190. DOI: 10.1016/j.jnucmat.2017.11.036.

27. Chen X., Li J., Cheng X., Wang H., Huang Z. Effect of heat treatment on microstructure, mechanical and corrosion properties of austenitic stainless steel 316L using arc additive manufacturing. *Materials Science and Engineering: A*, 2018, vol. 715, pp. 307–314. DOI: 10.1016/j.msea.2017.10.002.

28. Martyushev N.V., Kozlov V.N., Qi M., Tynchenko V.S., Kononenko R.V., Konyukhov V.Y., Valuev D.V. Production of workpieces from martensitic stainless steel using electron-beam surfacing and investigation of cutting forces when milling workpieces. *Materials*, 2023, vol. 16, p. 4529. DOI: 10.3390/ma16134529.

29. Shlyakhova G.V., Bochkareva A.V., Barannikova S.A., Zuev L.B., Martusevich E.V. Application of atomic force microscopy for stainless steel microstructure study at various kinds of heat treatment. *Izvestiya vysshikh uchebnykh zavedenii. Chernaya Metallurgiya = Izvestiya. Ferrous Metallurgy*, 2017, vol. 60 (2), pp. 133–139. DOI: 10.17073/0368-0797-2017-2-133-139. (In Russian).

30. Haidorov A.D., Yunusov F.A. Vakuumnaya termicheskaya obrabotka vysokolegirovannykh korrozionnostoikikh stalei [Vacuum heat treatment of high alloy corrosion-resistant steels]. *Nauchno-tekhnicheskie vedomosti Sankt-Peterburgskogo gosudarstvennogo politekhnicheskogo universiteta = St. Petersburg polytechnic university journal of engineering sciences and technology*, 2017, vol. 23 (1), pp. 226–235. DOI: 10.18721/JEST.230123.

31. Kondrakhin V.P., Martyushev N.V., Klyuev R.V., Sorokova S.N., Efremenkov E.A., Valuev D.V., Mengxu Q. Mathematical modeling and multi-criteria optimization of design parameters for the gyratory crusher. *Mathematics*, 2023, vol. 11, p. 2345. DOI: 10.3390/math11102345.

32. Yelemessov K., Baskanbayeva D., Martyushev N.V., Skeeba V.Yu., Gozbenko V.E., Karlina A.I. Change in the properties of rail steels during operation and reutilization of rails. *Metals*, 2023, vol. 13, p. 1043. DOI: 10.3390/met13061043.

33. Ahmetshin R., Fedorov V., Kostikov K., Martyushev N., Ovchinnikov V.A., Razin A., Yakovlev A. Capabilities of laser printers with different power. *Key Engineering Materials*, 2016, vol. 712, pp. 246–250. DOI: 10.4028/www.scientific.net/KEM.712.246.

Conflicts of Interest

The authors declare no conflict of interest.